Paper No.
7800

NACE INTERNATIONAL CORROSION 2016 CONFERENCE & EXPO

Using predicted corrosion damage to determine stress concentration, fracture and crack growth

Sharon Mellings, Andres Peratta, John Baynham, Tim Froome

CM BEASY Ltd

Ashurst Lodge Southampton, SO40 7AA, UK

ABSTRACT

Structure surfaces damaged by corrosion may develop stress concentrations which lead to initiation of cracks and possible crack growth.

Simulation of the galvanic effects leading to corrosion takes account of the properties of the electrolyte as well as the structural materials, to determine electric fields within the electrolyte, attenuation in the return path, and the surface current densities and potentials. If dissimilar materials are present or a CP system is not adequately designed, areas may exist where anodic current occurs on a structural surface, causing mass loss from the surface. The magnitude of the anodic current density, determined from simulation, can be used to determine surface shape change.

Such shape change generally results in indentations, which act as stress-raisers. Simulation to determine magnitude of the stress concentration can identify likely sites for crack initiation. The possibility of crack growth, and the time taken for the growth, can be determined using fracture and crack growth simulation.

This paper explores the combined use of galvanic simulation and fracture/crack growth simulation.

Firstly galvanic simulation is used to investigate the influences of parameters, including electrolyte thickness and conductivity, on rate of corrosion for a galvanic cell caused by a metallic sample in contact with a more noble material. The paper reaches conclusions regarding the type of environment that is likely to produce higher penetration rates and where this might occur.

Secondly, having removed material from the surface (corresponding to corrosion occurring over a given time), fracture simulation is used to evaluate the stress concentration, initiate cracks, determine stress intensity factors, and identify vulnerability to fatigue failure. This crack growth takes into account the corrosion damage and inherently includes local stress

concentration due to the damaged surface. In the crack growth simulation, the full crack path and direction are determined along with the fatigue life.

This paper provides a methodology that can be used by design engineers, to identify possible problems on a structure, giving scope to change designs and so reduce possible failures and in-service repair costs. This methodology identifies areas of the structure that have the greatest risk of damage - which may not be obvious without combined corrosion and fracture simulation; and so provides more informed targeting of locations where “what if” fracture mechanics assessments should be applied.

Key words: Corrosion damage, stress concentration, crack growth

INTRODUCTION

If a structure develops corrosion damage, this damage leads to stress concentrations within the structure, and these elevated stresses increase the likelihood of initiation and growth of cracks. Even a thin film of electrolyte on the surface of the structure can lead to an electrical field that causes surface damage.

Computation of the electrical field within the electrolyte can be used to identify areas of the structure that are most susceptible to corrosion damage and which, after possible crack initiation and fatigue crack growth, may lead to structural failure. Corrosion simulation can be used to take account of the properties of the electrolyte as well as the structural materials, to determine the rate of material loss from the structure. Having removed material from the surface (corresponding to corrosion occurring over a given exposure time) the stress concentrations can be evaluated and, if required, cracks can be initiated in each possible problem area, to identify vulnerability to fatigue failure.

Different extents of corrosion damage are likely to arise when different electrolytes are present, for example parts of structures operating above sea level may be subjected to salt water spray which produces a thin film of electrolyte (on the surface of the structure) through which oxygen may be readily able to diffuse. A structure immersed in the sea is surrounded by electrolyte and rates of diffusion of oxygen are likely to be lower.

Simulation of the galvanic effects leading to corrosion has been successfully used for many years to assist design of cathodic protection systems for marine vessels and offshore structures, and has more recently been applied to structures which are not immersed.

This paper is focused on the modelling of a typical test specimen exposed to a corrosive environment and subject to cyclic fatigue load, which can lead to the initiation and propagation of cracks.

This paper is in two parts. Firstly, the galvanic corrosion modelling of the specimen exposed to thin films and deep layers of electrolyte is presented and discussed. Secondly, the corrosion damaged specimen, after initiation of cracks, is subjected to a fatigue load, with corresponding crack propagation presented.

This type of simulation (combined corrosion and fracture) is likely to be relevant to diverse structures such as ships, offshore jackets, subsea infrastructure and so on.

CORROSION MODELING

Introduction

BEASY† software has been used in this paper to simulate galvanic effects for a structurally loaded test specimen exposed to electrolyte. The simulation determines electrical fields in the electrolyte and current densities on the wetted surfaces of the specimen. As the specimen includes dissimilar materials (a “stretch part” made of aluminum alloy and “clamps” made of a carbon-fiber reinforced plastic as shown in Figure 1) the simulation predicts the rate of corrosion of the aluminum alloy.

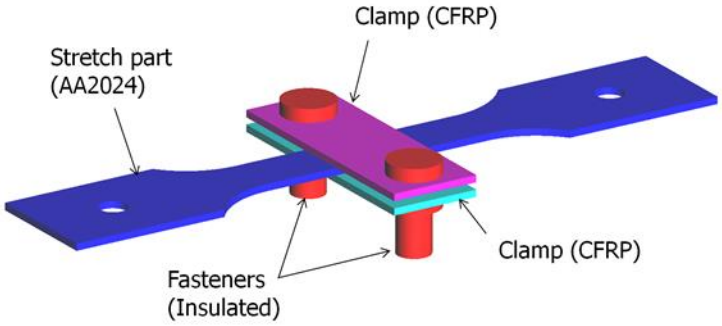

Figure 1. Test specimen used for corrosion modelling.

The stretch part is assumed to be perfectly electrically connected to the clamps, and it is assumed that internal electrical resistance of the two parts is negligible. Internal resistance in the return-path (either in the components or caused by mechanical contact) tends to reduce the flow of current through the electrolyte. This could be important in some situations, in which case such effects should be included in the simulation. Because of the dissimilar electrochemical nature of the materials involved, a corrosion cell develops between the two components whenever the specimen is exposed to an electrolyte. The material of the clamps is more electrochemically noble than that of the stretch part, which means that the latter will corrode. In other words, the stretch part will behave anodically, the clamps will behave cathodically, and an ionic current (driven by the different polarisation properties of the coupled materials) will flow through the electrolyte. Corrosion damage occurs in the anodic region, and the distribution of normal current density flowing from the anodic surface into the electrolyte is a direct measure of the rate of damage, as expressed by equation (1) which is based on Faraday’s law.

$$CR = B_1 \frac{j_n}{\delta} EW \tag{1}$$

where:

CR = Corrosion rate, expressed in mm/year.

j_n = Corrosion current density, expressed in A/m^2

δ = Mass density, in kg/m^3

EW = Equivalent weight of the corroding sample (see below)

† Trade name.

B1 = Constant involving Faraday's constant and unit conversion factors such that the result appears in mm per year. The value of B1 is 327.2 mm kg/(A m yr)

The specific mass loss rate (SR) is related to j_n by the expression $S_R = B_2 j_n EW$ where B_2 is a constant involving Faraday's constant and unit conversion factors, K2 = 895.3 mg/(A day), so that SR is expressed in mg/(day m^2).

The mass loss rate for an entire component can be expressed as:

$$M_R = B_2 \times I \times EW \tag{2}$$

where I is the total anodic current for the component, and M_R is expressed in mg/day

The equivalent weight ("EW") for an alloy can be calculated as follows:

$$EW = \frac{1}{\sum_i \frac{n_i \phi_i}{W_i}} \tag{3}$$

where:

Φi = mass fraction of the i-th element in the alloy

Wi = atomic weight of the i-th element in the alloy expressed in grams per mol

ni = the number of electrons involved in the oxidation process of the i-th element in the alloy

Using the above expression, the equivalent weight for the aluminum alloy stretch part is calculated to be 9.38.

The form of the electric field in the electrolyte is affected by the geometry of the polarising surfaces, the polarisation curves, the geometry of the electrolyte, electrical properties of the electrolyte, and if appropriate any electrical resistances in the return-path through the conducting solid structures.

Simulation of the electrochemical effects involves solution of the Laplace equation in the electrolyte with non-linear boundary conditions representing the influence of the polarisation curves for the wetted surfaces. If the electrolyte is a thin film coating the surfaces of the structures (for example condensation or spray), it is treated as a two dimensional domain warped in three-dimensional space to follow the geometry of the structures. The background for corrosion modelling can be found in [1 - 5] and references therein.

Modeling Assumptions

Figure 2 shows the geometry and dimensions of the test specimen, which includes a "stretch part", held between two "clamps" by bolts which are assumed to be perfectly coated (so they are insulated from the electrolyte). The stretch part is made of aluminum, and the clamps of a very noble carbon fiber material.

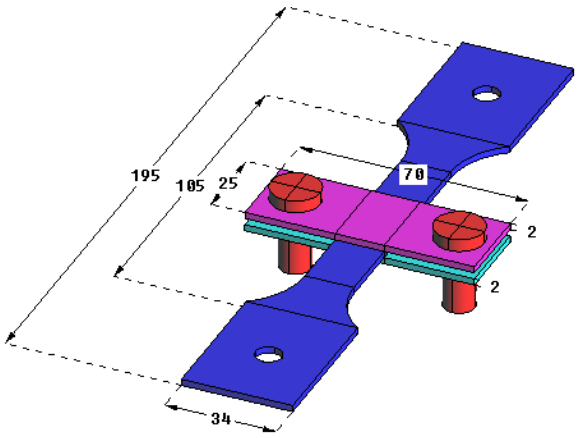

Figure 2. Specimen dimensions (in millimetres).

Unless specified otherwise, the electrolyte is a saline solution of 0.3M NaCl with conductivity 0.5 S/m. The polarisation properties used in this study for the aluminum (AA2024-T3) and the carbon fiber (CFRP) are shown in Figure 3. These curves were derived from work reported in [10].

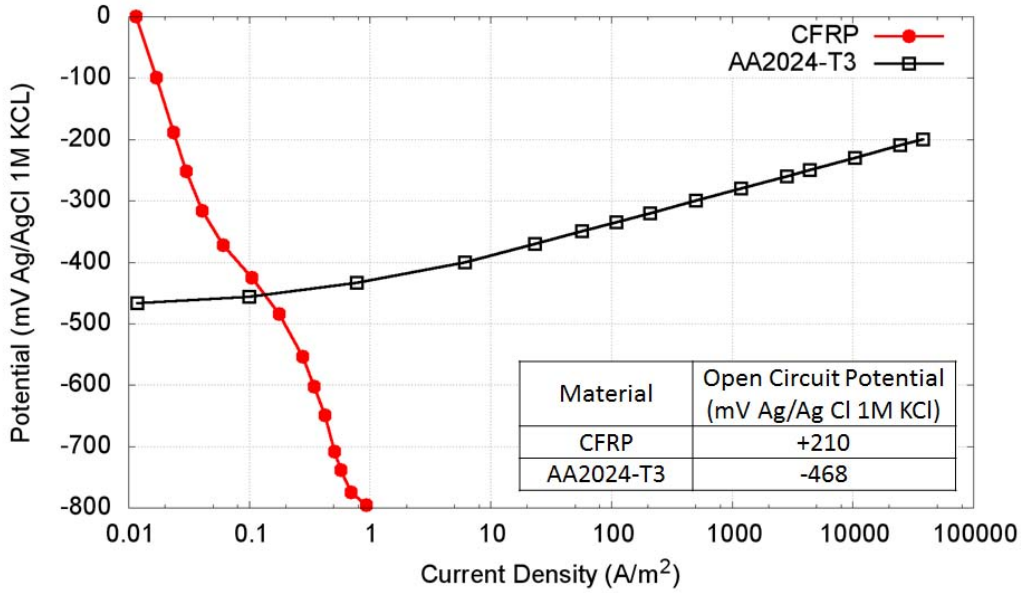

Figure 3. Polarisation curves.

Unless otherwise indicated, potentials are in Volts relative to the Ag/AgCl (1M KCl) reference electrode; currents are expressed in Amperes, and current density in Amperes per square metre.

Case 1: A deep volume of electrolyte

In this case, the specimen is immersed at the centre of a 'large' (2m x 2m x 2m) volume of electrolyte in a tank with perfectly insulated surfaces. Because the dimensions of the tank are big compared to the specimen, the solution obtained is representative of a sample submerged in an infinitely large volume of electrolyte.

The distribution of polarisation potential on the cathodic and anodic regions is shown in Figure 4. The polarisation potential ranges approximately from about -0.438 V to -0.460V (a difference of about 22 mV).

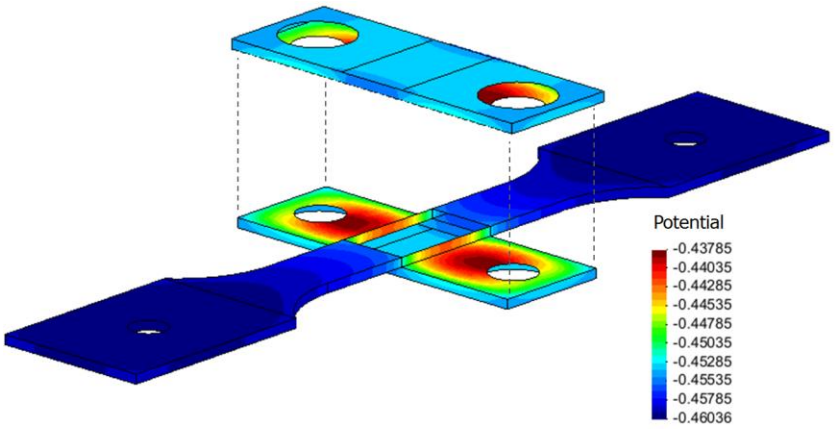

Figure 4. Contours of polarisation potential (u) in Volts on anodic and cathodic surfaces.

Figure 5 shows the distribution of normal current density on wetted surfaces of the aluminum part and the bottom clamp. The aluminum part behaves entirely anodically and the current density ranges from about 0.07 A/m^2 to about 0.53 A/m^2. The biggest value of anodic current density occurs on the side of the stretch part between the two clamps, while the smallest occurs on the areas most distant from the clamps. The cathodic current density (on the clamp) is comparatively more uniformly distributed and averages about 0.12 A/m^2.

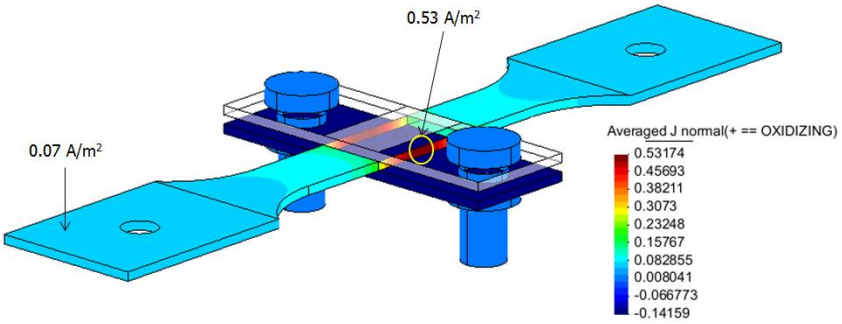

Figure 5. Contours of normal current density (jn) in A/m^2 on anodic and cathodic surfaces (here a positive current density indicates anodic behaviour).

The current flowing between the aluminum part and the clamps is about 0.81 mA, which corresponds to a mass loss rate of 6.8 mg/day.

Case 2: A thin film of electrolyte

Various film thicknesses were used in parameter studies (see Figure 9), but in the example shown, a 100 μm thick film was assumed, covering the clamps and the aluminum part. Figure 6 shows the resulting distribution of polarisation potential, which ranges from -0.157 V to -0.468 V (a difference of 311 mV).

Figure 7 shows the corresponding distribution of normal current density using two different scales, one for the cathodic currents on the clamps (with negative values), and the other for the anodic currents on the stretch part (with positive values). The biggest anodic current

density (approximately 3.4 A/m^2) occurs at the edges of the stretch part in contact with the clamps, and it rapidly decays to nearly zero in all regions of the aluminum more distant than 20mm from the clamps.

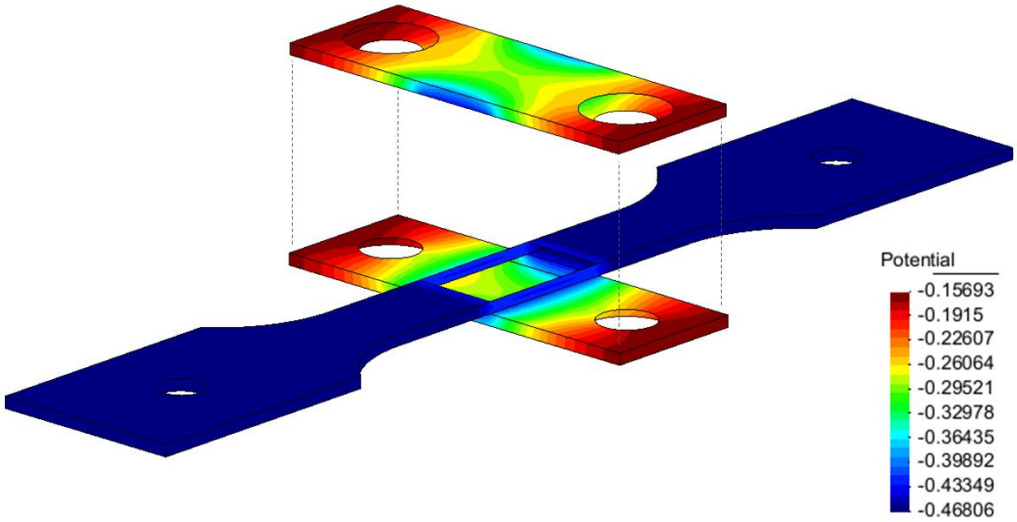

Figure 6. Contours of polarisation potential (u) in Volts on the wetted surfaces of the specimen exposed to thin film.

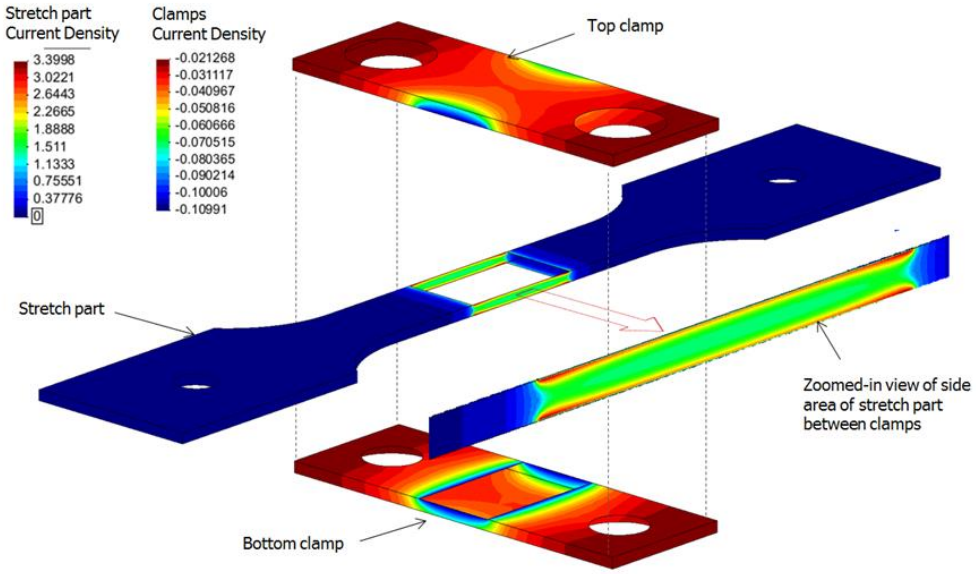

Figure 7. Contours of normal current density (jn) in A/m^2 on the surfaces of the specimen exposed to a thin film electrolyte (of thickness 100 μm).

Figure 8 shows the distribution of corrosion rate on the section of the stretch part with highest anodic current density, and vectors showing the electric field direction in the thin film of electrolyte.

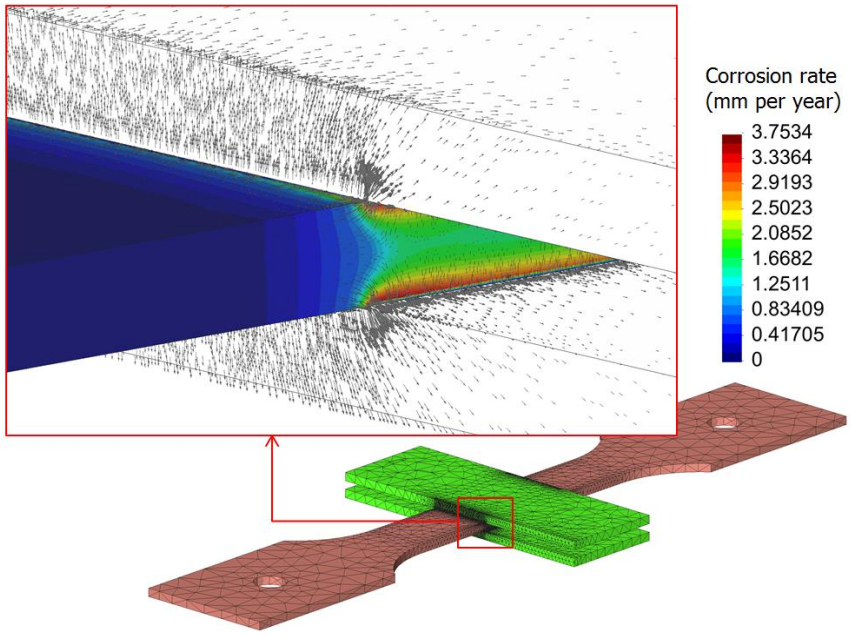

Figure 8. Contours of corrosion rate on the area of the stretch part with biggest anodic current density. The arrows represent electric field in the electrolyte.

The current flowing between the aluminum part and the clamps is about 0.2mA, which corresponds to a mass loss rate of about 1.73 mg/day.

Several cases were solved to determine how the mass loss rate changes with electrolyte thickness, and the result is shown in Figure 9. Figure 10 shows how the mass loss rate, calculated for increasing values of electrolyte thickness, tends to the limiting value for the deep electrolyte.

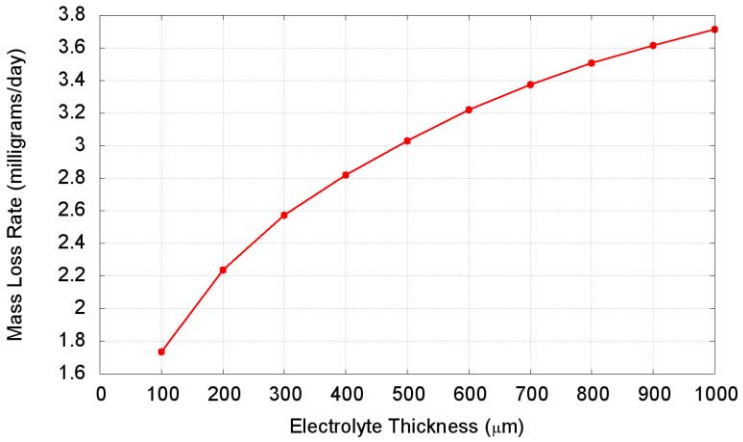

Figure 9. Variation of total mass loss in the stretch part as a function of electrolyte thickness.

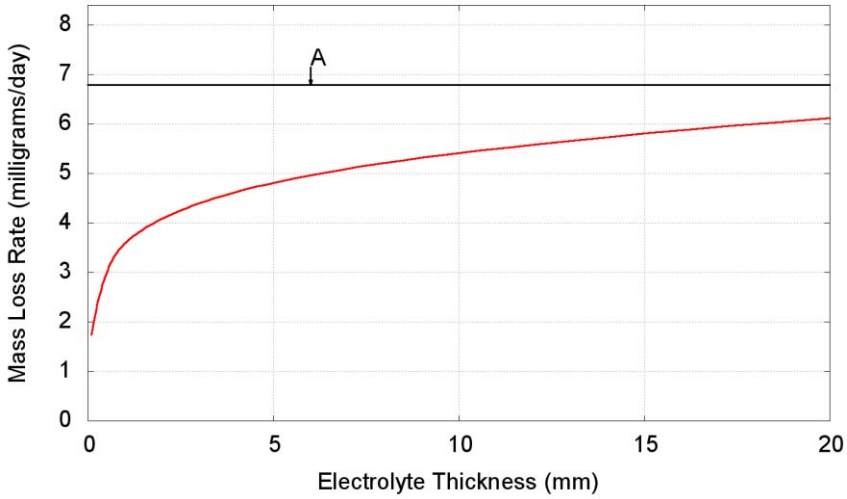

Figure 10. Showing mass loss rate as a function of electrolyte thickness. Line (A), indicating mass loss rate = 6.8 mg/day, corresponds to the result obtained for the specimen immersed in a large pool of electrolyte.

To take account of mass loss due to anodic dissolution, the position of each mesh point was changed by a translation proportional to the corrosion penetration rate (determined using the thin-film results) and directed along the normal to the sample surface. A further solution was obtained and the process repeated until the geometry of the specimen damaged by corrosion eventually took the form shown in Figure 11 after a certain period of corrosion. It was assumed that the polarisation properties of the aluminum surface remain the same during this process – in other words it was assumed that localized pitting does not occur and mass loss is uniform.

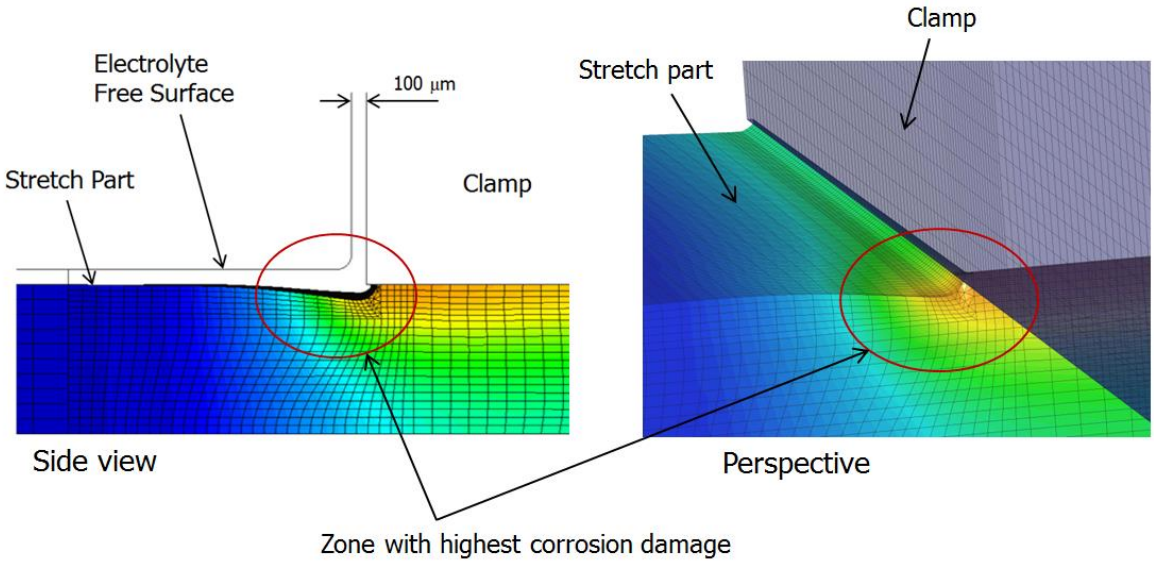

Figure 11. Showing geometry changes in the specimen due to corrosion damage.

STRESS CONCENTRATION RESULTING FROM CORROSION DAMAGE AND CRACK GROWTH

As discussed earlier, corrosion results in loss of material from an affected structure. This leads to localized stress concentrations, which can accelerate development and growth of cracks and fatigue failure of the part. Using the corrosion simulation results, a prediction of material loss after a given time has been determined and used to modify the geometry of the part prior to computation of the stress concentrations.

Having identified the areas of greatest stress concentration, cracks were initiated in the component at these positions using an automatic crack modelling tool. Crack growth simulation was then performed, growing these cracks automatically using fatigue crack growth, under cyclic loading.

Since the geometry used for the stress analysis includes corrosion damage in the "un-cracked" model, the crack growth simulation intrinsically takes account of the effects of the corrosion damage. This incorporates stress concentrations due to the material loss directly within the crack growth simulation, rather than requiring any numerical correction in the computed fatigue results.

Stress concentration due to the corrosion damage

The corrosion simulation showed that the greatest susceptibility to corrosion damage is at the interface between the carbon fiber and the aluminum. This crack growth example therefore assumes corrosion damage in the form of a 0.15mm deep notch *across* the part as shown in Figure 12. Such surface damage is ideally suited to stress analysis solution using boundary element modelling and it would be possible to simulate any damage that is predicted by the corrosion simulation.

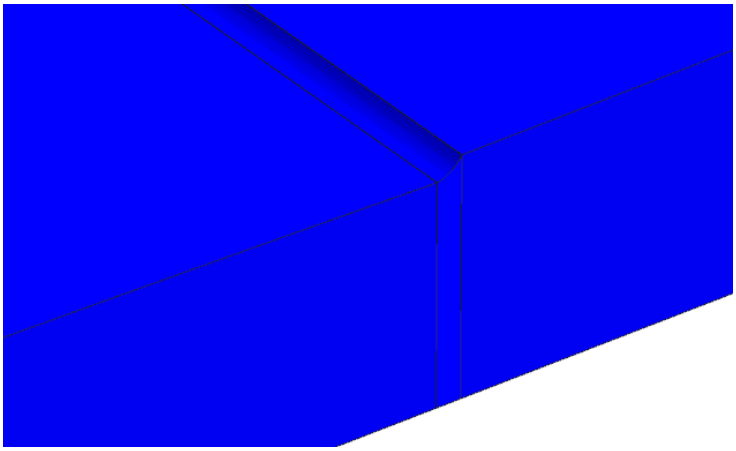

Figure 12. Damaged stretch component.

The stretch part was subjected to a nominal uniaxial load of 50.2N, applied using a traction on one of the bolt holes with the other bolt hole clamped. In addition normal restraint was applied to the central section where the clamps restrict out of plane deformation of the stretch part.

Resulting stresses are shown in Figure 13 and Figure 14.

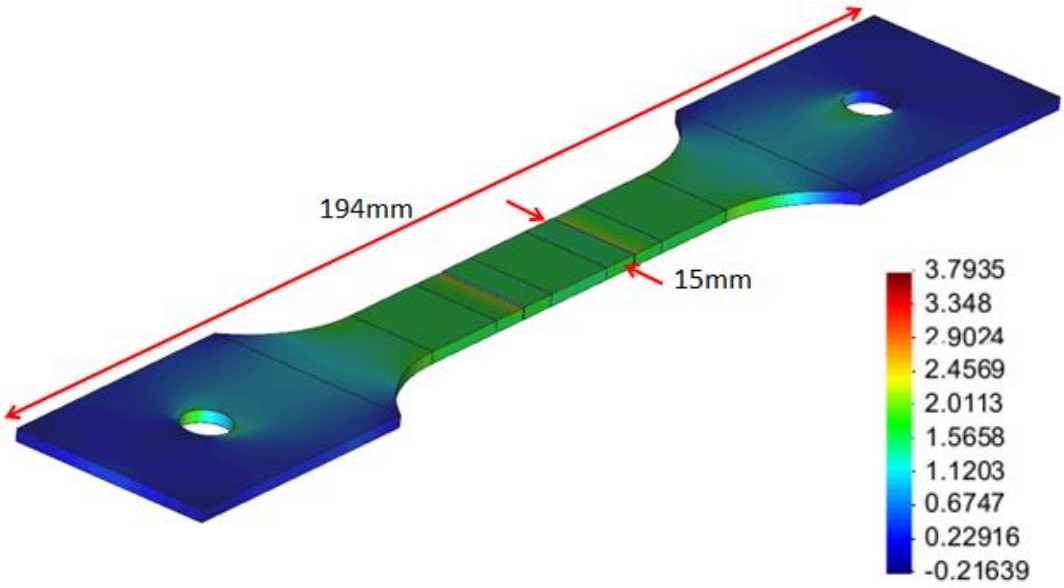

Figure 13. Maximum principal stress (MPa) on the damaged stretch component.

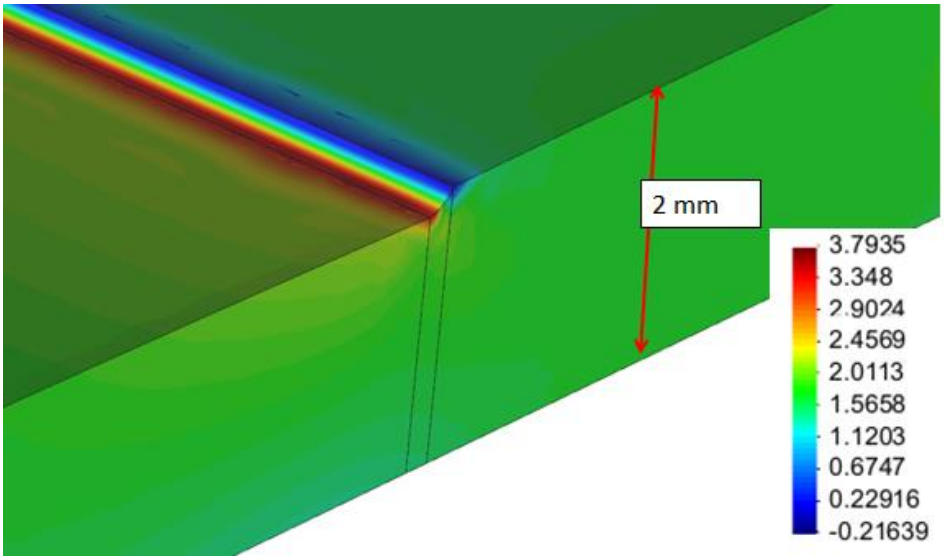

Figure 14. Localized maximum principal stress (MPa) on the damaged stretch component.

The results show a peak stress concentration factor of 2.52 at the bottom of the notch, indicating that the bottom of the notch is a likely location for crack initiation.

Crack analysis with a single edge crack

The highest stress value occurred at the bottom of the corrosion damage, a short distance from the corner of the part. In addition to increasing the likelihood of crack initiation (by virtue of the increased stress) the damaged shape of the structure may also affect the rate and direction of crack growth. It is therefore generally preferable to simulate crack growth in a damaged part.

The damaged model shown in Figure 12 has been used for crack growth simulation, using a surface edge crack of radius 0.1mm, initiated at the point where the highest stress concentration occurred in the notch.

The stresses were determined using the Dual Boundary Element Method [6-9]. Resulting stresses and stress intensity factors (SIFs) are shown in Figure 15 and Figure 16.

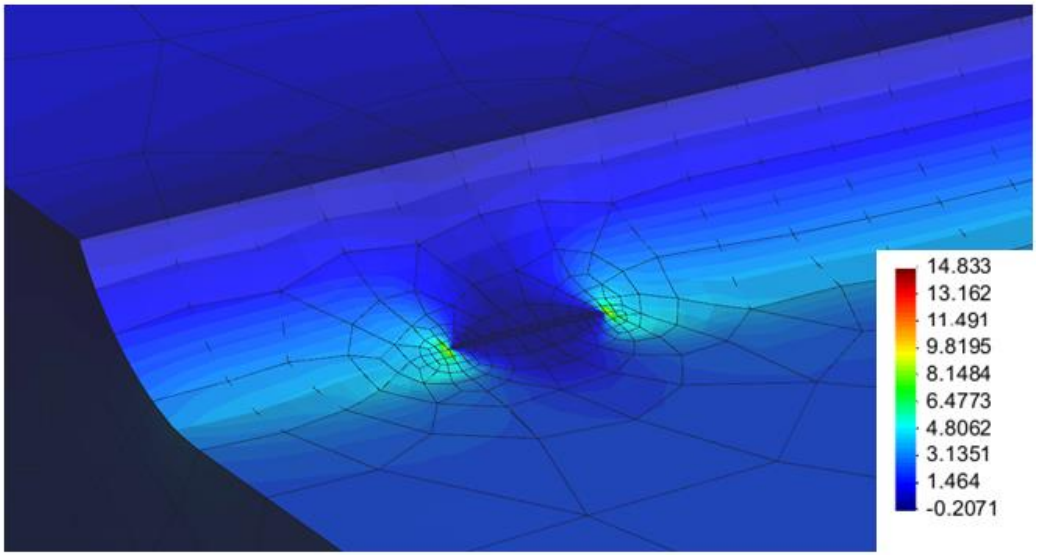

Figure 15. Maximum principal stress (MPa) near the initial edge crack.

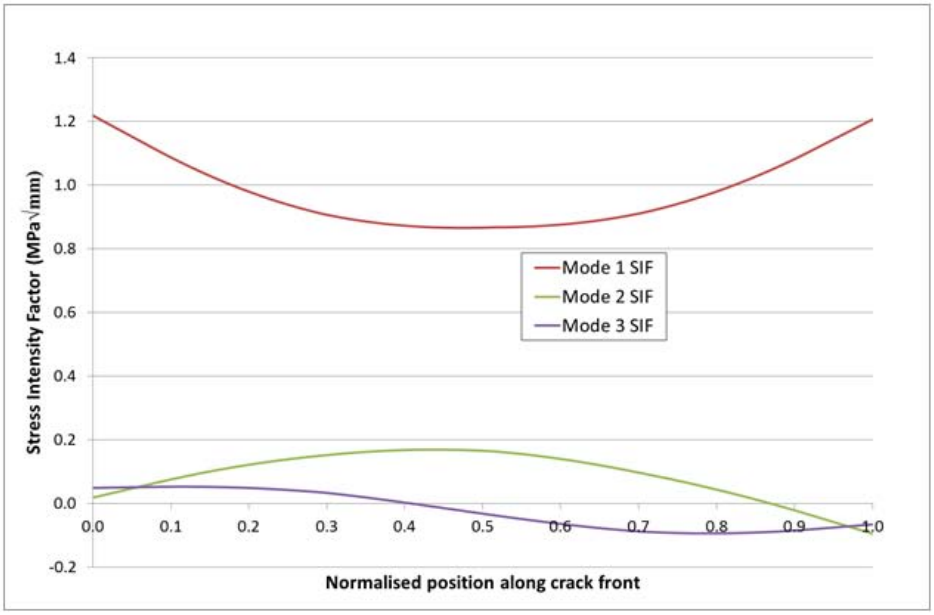

Figure 16. Variation along the crack front of stress intensity factors caused by the nominal uniaxial load

Fatigue crack growth of a single edge crack

The stress intensity factors which result from the nominal applied load of 50N are not sufficiently high to cause the crack to start growing (assuming cyclic loading from zero to 50N and back to zero). However such results are typically used to determine the effects of different load scenarios, which could include combined multi-axial loading or complex loading histories, generally defined using a load spectrum which identifies load multipliers and ranges of the cyclic loading.

In this example, we assumed that the crack is subject to a fatigue load cycling between 0 and 7500N, by means of a load factor of 150. Since the stretch part is assumed to have linear

elastic properties, the SIF values for the increased load can be determined by scaling the values obtained for the "nominal" load. If a structure is subject to several different load cases combined in different ways, the resulting effect can be determined by appropriately combining the SIF values from each of the load cases.

In this work the fatigue crack growth was performed assuming no influence (beyond creation of the initial damage) of corrosion on the growth of the crack.

Using this load regime in conjunction with a set of NASGRO 3.0[†] fatigue properties for an aluminum material, the crack has been grown automatically, re-computing the SIF values periodically during the crack growth.

After a number of automatic growth increments, the edge crack reached and grew around the corner of the structure (as shown in Figure 17), and then continued to grow more quickly through the thickness of the specimen.

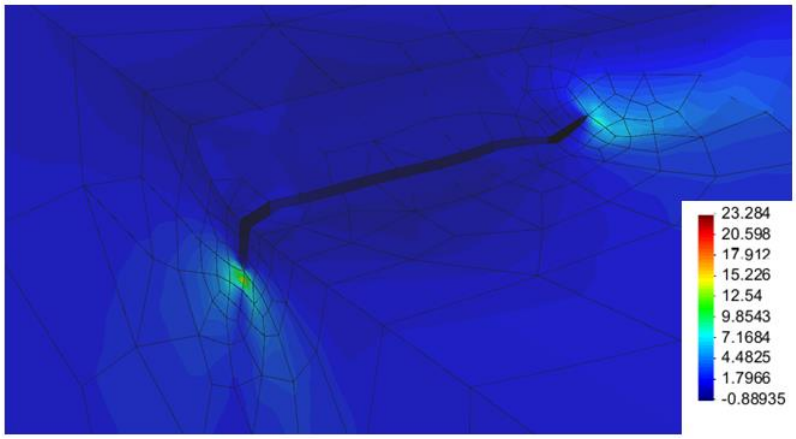

Figure 17. Maximum principal stress (MPa) after the crack has grown around the corner

The crack growth simulation was continued, with the stresses and SIFs re-computed at every stage. After a number of additional growth steps the crack reached and grew around the bottom corner, and became a “through crack” as shown in Figure 18. The variation of crack size with the number of load cycles (the “life” of the crack) is shown in Figure 19.

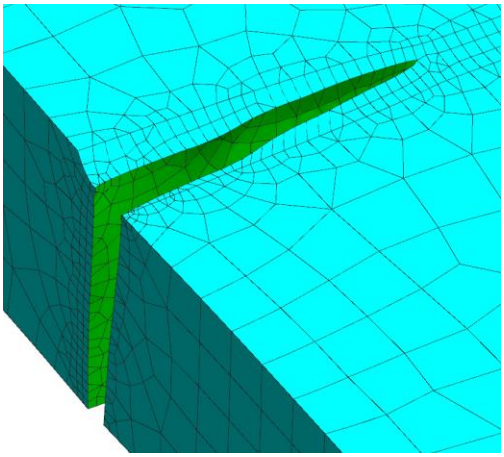

Figure 18. Crack after transition to a through crack.

[†] Trade name.

When a crack of the same initial size and position was assumed in the un-corroded structure and subject to the same loading, the stress intensity factors were such that the crack would not grow, as shown by the horizontal red dashed line in figure 19.

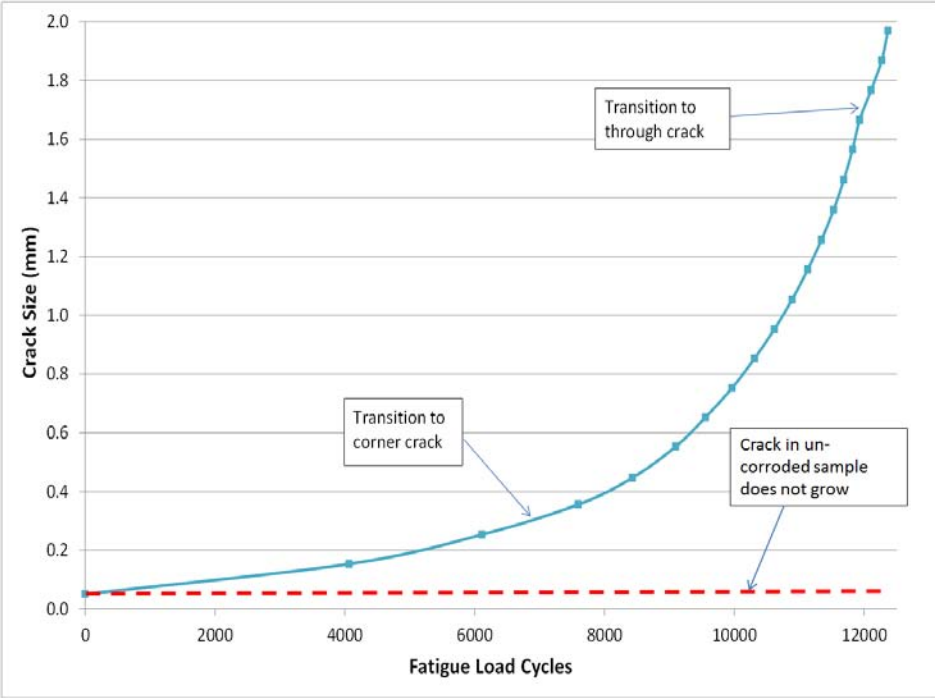

Figure 19. Fatigue results for growth of the crack.

SUMMARY

The damage caused by galvanic corrosion and subsequent mechanical loading of a specimen consisting of two dissimilar materials exposed to different types of electrolyte has been quantified using a computational modelling approach based on boundary element software.

The corrosion simulation can predict mass loss rate, corrosion penetration rate, current density, electric fields and polarisation potentials on the specimen exposed to different types of electrolytes. With fatigue loading of the corrosion-damaged part, simulation can be used to grow an initial crack to failure (or example when the stress intensity factors reach the critical value at which catastrophic fracture occurs), and can determine the number of loading cycles to reach failure.

An example of an aluminum stretch part in between two CFRP clamps has been solved for different environmental conditions.

The corrosion damage resulting from anodic dissolution caused a geometry change in the aluminum, which affected the distribution of mechanical stress and subsequent crack propagation.

Although the example shown assumed no changes of polarisation properties with mass removal, it is possible that loss of surface films could lead to locally changed properties (for some materials), and accelerated corrosion such as pitting.

The example shown is for specific materials (CFRP and AA2024) and specific geometry and electrolyte. Nevertheless, the results support the following general observations:

- The galvanic effects observed with exposure to a thin film of electrolyte can cause much higher penetration rates than in the case of deep electrolyte.
- The distribution of anodic current density (and therefore corrosion damage) becomes significantly more localized as the thickness of the electrolyte decreases. In general, when the sample is exposed to thin films, the corrosion damage tends to accumulate at the edges near the junctions between dissimilar materials, whereas for bulk electrolytes, the damage becomes more uniformly distributed, extending to farther regions.
- Assuming no changes of the concentration of oxygen in the electrolyte, or of the polarisation curves of the materials involved, the overall mass loss rate in the case of fully immersed samples is always bigger than in the case of exposure to a thin film. This is because the electrical resistance through the electrolyte is increased when the electrolyte thickness decreases.
- As the film thickness increases, the overall mass loss rate obtained with a thin film of electrolyte tends to the value obtained for the sample in a large tank of electrolyte.

REFERENCES

1. R. Adey and S. Niku (1988). In: Galvanic Corrosion, ASTM Committee G-1 on Corrosion of Metals, Hack, H. (Ed.), ASTM International.
2. P. Roberge, “Corrosion Engineering. Principles and Practice”. McGraw-Hill 2008.
3. A. Peratta, T. Hack, R. Adey, J. Baynham, H. Lohner, “Galvanic Corrosion Modelling for Aircraft Environments”, Eurocorr 2009, Nice.
4. A. Peratta and R. Adey, “Modeling Galvanic Corrosion in Multi-Material Aircraft Structures”, NACE Corrosion 2013.
5. S. Palani, T. Hack, A. Peratta, R. Adey, J. Baynham, H. Lohner, “Validation Of A Galvanic Corrosion Model For AA2024 And CFRP with Localised Coating Damage”. Eurocorr 2010.
6. A. Portela, M. Aliabadi, D. Rooke, “The Dual Boundary Element Method: Efficient Implementation for Cracked Problems”, *International Journal for Numerical Methods in Engineering*, 32 (1992): pp. 1269-1287.
7. Y. Mi, M. Aliabadi, “Three-dimensional crack growth simulation using 6EM”, *Computers & Structures*, 52 No. 5, (1994): pp. 871-878.
8. S. Mellings, J. Baynham, R. Adey, “Advances in crack growth modelling of 3D Aircraft Structures”, International Committee on Aeronautical Fatigue, Rotterdam, Netherlands, May 2009.
9. R. Rigby, M. Aliabadi, “Decomposition of the mixed-mode J-integral—revisited”, *International Journal of Solids and Structures*, 35 Issue 17 (June 1998): pp. 2073-2099.
10. J. DeRose, T. Suter, T. Hack and R. Adey, *Aluminium Alloy Corrosion of Aircraft Structures: Modelling and Simulation*, (Southampton, UK: WIT Press, 2013), subsection 3d p.95.